Measuring tilt and focus for sodium beacon adaptive optics on the Starfire 3.5 meter telescope

Robert L. Johnson
Air Force Research Laboratory, Directed Energy Directorate
Starfire Optical Range, Kirtland Air Force Base, New Mexico

ABSTRACT

Adaptive optics systems can measure high-order aberrations using an artificial laser beacon without the need for a relatively bright object near the object being imaged. Unfortunately, tilt and focus measurements are difficult to obtain from a laser beacon. One solution is to use light from the object being imaged to measure tilt and focus. Through analysis, I estimate the performance of using a Shack-Hartmann wavefront sensor with 2 by 2 sub-apertures for measuring tilt and focus. Specifically, I discuss implementing this scheme for the sodium beacon adaptive optics upgrade to the Starfire Optical Range (SOR) 3.5 m telescope. I use wave-optics simulation tools to evaluate the performance of the tilt and focus sensor in the SOR sodium beacon system.

1. INTRODUCTION

When employing a sodium laser beacon in an adaptive optics system, one can not use tilt or focus measured from the beacon to correct images of an object above the Earth's atmosphere. Tilt from the beacon can not be used, because the tilt on the outgoing path is not the same as the tilt on the incoming path. This is (potentially) because of jitter on the outgoing beam caused by vibration in the telescope. To make matters worse, focus from the beacon can not be used, because the altitude of the sodium layer may vary spatially and temporally. In addition, when imaging an Earth-orbiting satellite from a land-based telescope, the range to the satellite varies with telescope elevation angle and hence with time (except perhaps, for satellites in Clarke orbits).

One solution to this dilemma is to use light from the object itself to measure tilt and focus, as in the Keck adaptive optics system. [1] We chose a similar approach for the planned upgrade for the Starfire Optical Range (SOR) 3.5 m telescope sodium guide-star adaptive optics system. A small amount of the light from the object is redirected from the imaging optical path to a small Shack-Hartmann wavefront sensor with 2×2 subapertures. We will use this device, called the tilt and focus sensor, to provide an absolute measure of tilt and focus for the object.

In this paper, I discuss our preliminary design and include a brief description of a wave-optics simulation of the tilt and focus sensor. This simulation does not include atmospheric turbulence effects. To check the simulation in a well-understood application, I used the simulation to model a typical quad-cell tracker. I then applied the simulation to the tilt and focus sensor to explore the range of measurement for tilt and focus, cross-coupling of measurements, and errors in measurements in the presence of noise. Lastly, I make suggestions for further work.

2. FOCUS MEASUREMENT AND CONTROL APPROACH

In the SOR 3.5 m telescope sodium guide-star adaptive optics system, focus measured from the beacon will be used for high-bandwidth focus correction, while focus measured from the object will be used for low-bandwidth focus correction. This concept is illustrated in Figure 1. The amount of focus sensed by the sodium beacon wavefront sensor includes high-bandwidth focus errors introduced by the atmosphere, and low-bandwidth focus errors introduced by changes in range to the sodium layer.

The tilt and focus sensor will be used to drive a fast steering mirror to control overall wavefront tilt (not shown in the diagram for clarity). In addition, the tilt and focus sensor will be used to drive a linear translation stage that is part of an optical trombone upstream of the sodium beacon wavefront sensor. The purpose of this stage is to adjust for the difference in focus between the object and the sodium beacon. Movement of this stage causes focus to be sensed by the sodium beacon wavefront sensor, which drives the deformable mirror to correct this focus. Large amounts of focus are corrected by moving the secondary mirror of the telescope in a very low-bandwidth correction loop. In other words, focus is off-loaded from the deformable mirror to the secondary mirror.

To help understand how this arrangement works, imagine that all control loops are closed, there is no focus sensed by either the sodium beacon wavefront sensor or the tilt and focus sensor, and the deformable mirror is adjusted to provide zero focus. Then imagine there is a small change in range to the sodium layer. This causes focus to be sensed by the sodium beacon wavefront sensor which commands the deformable mirror to remove this focus. This, in turn, causes a focus error to be sensed by the tilt and focus sensor, which is observing light from the object. The tilt and focus sensor drives the optical trombone to introduce the right amount of focus into the sodium beacon wavefront sensor path to cause the deformable mirror null the focus it observes. The net result is the sodium beacon wavefront sensor and tilt and focus sensor observe no focus, the deformable mirror has zero focus applied and the optical trombone has been adjusted to account for the small change in range to the sodium layer.

This convoluted arrangement, along with a more straightforward approach, albeit a bit more complicated, are described in detail by Link and Foucault. [2] They show these approaches to focus control have comparable performance in the presence of atmospheric turbulence.

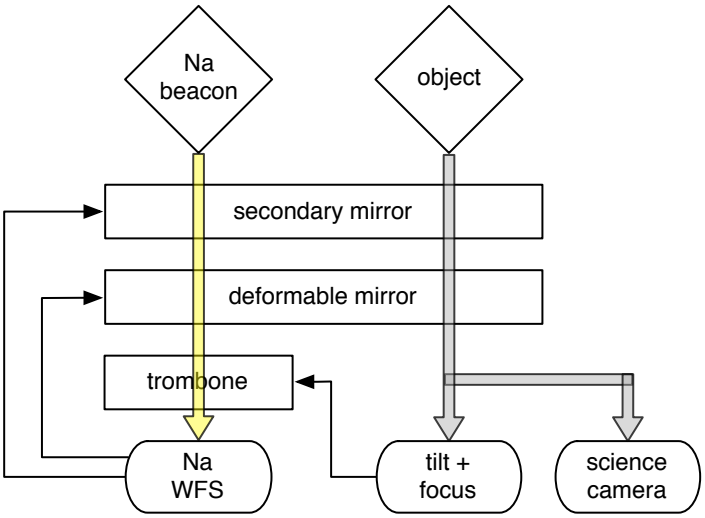

Figure 1. Focus measurement and control concept.

3. Simulation using Wave Optics Model

To simulate the performance of the tilt and focus sensor, I built a wave-optics model using wave optics techniques outlined in Goodman [3], which were applied to a Shack-Hartmann wavefront sensor by Roggemann and Schulz [4]. The model first maps the phase at the telescope pupil to a lenslet array. The amplitude transfer function of the lenslet array is generated and is used to compute the field just after the lenslet array. This field is then propagated to a multi-element detector at the image plane of the lenslets. From this field, the intensity is calculated and binned to represent photoelectrons as sensed by the individual detector array elements or pixels. Shot noise and read noise can be added at this point. Since we are interested in measuring tilt and focus, I generated a simple least-squares modal reconstructor to extract the first 3 Zernike terms (excluding piston) [5] from the simulated detector output.

The parameters used as inputs to the model are listed in Table 1. Since the optical design for the tilt and focus sensor had not been completed when I ran these simulations, these parameters are not exactly the same as the system we will build, but they are representative. The prototype optical design includes two sets of optics, one that relays an image of the pupil to a lenslet array, and another that relays the spots formed by the lenslets to a detector array. These relay optics were not included in the model.

Table 1. Parameters used to describe tilt and focus sensor.

Parameter	Value
wavelength	0.65 µm
lenslet focal length	6 mm
lenslet width	200 µm
detector pixel width	50 µm
pixels per sub-aperture	4×4 pixels
guard band width	2 pixels

4. Results and Analysis

To check my simulation approach, I applied it to a well-understood application, a quad-cell tracker. Tyler and Fried derive the angular measurement error for a quad-cell tracker and an object with small angular extent as [6]

$$\sigma_\theta = \frac{3\pi}{16}\frac{\lambda}{D}\,\mathrm{SNR}^{-1} \tag{1}$$

where λ is the wavelength, D is the diameter of the pupil, and *SNR* is the signal-to-noise ratio, which is given by

$$\mathrm{SNR} = \frac{n_p}{\sqrt{n_p + N_D(n_B^2 + rn^2)}} \tag{2}$$

where n_p is the total number of photoelectrons for all pixels, N_D is the number of pixels, n_B is the number of detected background electrons (dark current plus sky background), and *rn* is the read noise in electrons. [7]

Figure 2 shows the angular measurement error versus detected signal, for theory and simulation for 2500 measurements using a quad-cell tracker. Parameters were for a single sub-aperture as listed in Table 1. The background noise was 0 and the read noise was 3 electrons. (It is unclear to this author why the theory and the simulation do not match at higher signal levels, although this is being examined.)

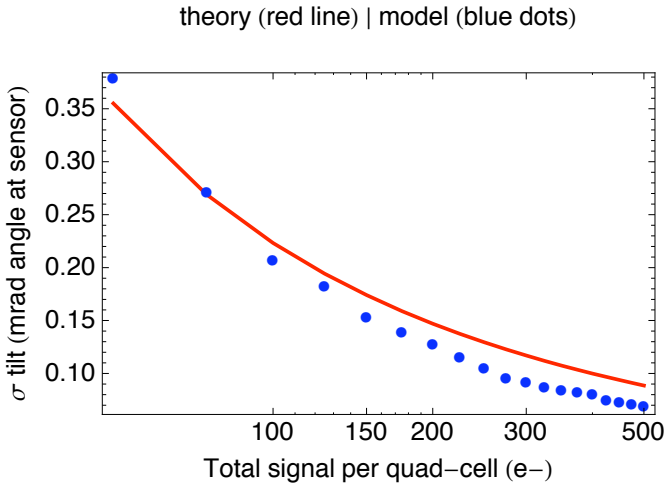

Figure 2. Angular tilt measurement error versus signal for a quad cell.

The signal-to-noise ratio, given in equation 2, is plotted in Figure 3. Here, the theory and the simulation match well.

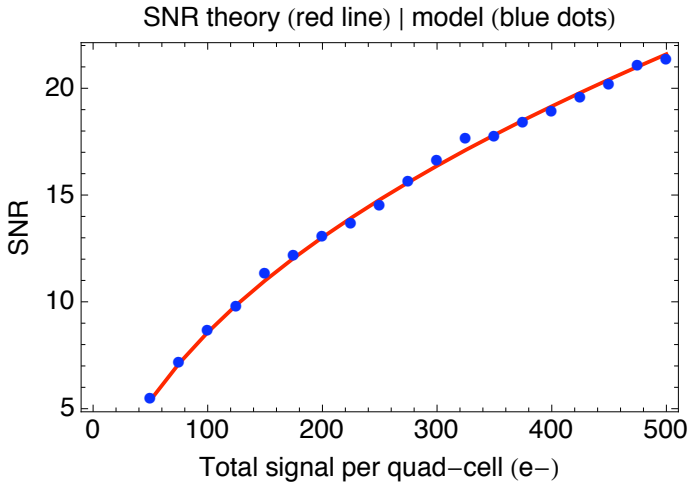

Figure 3. Signal-to-noise ratio versus signal for a quad cell with 3 electrons of read noise and 0 background noise.

In spite of the unexplained discrepancy between the theory and the model for the error in angular measurement with a quad-cell, I applied the model to the tilt and focus sensor, which is a 4 sub-aperture Shack-Hartmann wavefront sensor. First, I explored the coupling between tilt and focus by inserting known amounts of Zernike tilt and focus into the model and applying a least-squares modal reconstructor. Figure 4 shows the output of the modal reconstructor with varying amounts of Zernike x-tilt input to the model. In this case, there was no detector noise. Nearly identical results were obtained for y-tilt. Figure 5 shows a similar output for inserting focus, again, with no detector noise.

In both cases, the desired output is output by the model, up to a certain magnitude. As the input magnitude is increased, the response of the sensor tapers off or saturates. In other words, up to some value, the same amount of tilt or focus is measured as is inserted into the model. Tilt starts to saturate at about 0.15 µm rms wavefront, and focus starts to saturate at 0.10 µm rms wavefront. Also, when x-tilt is input, very little y-tilt or focus is measured. Similarly, when focus is inserted, very little tilt is measured.

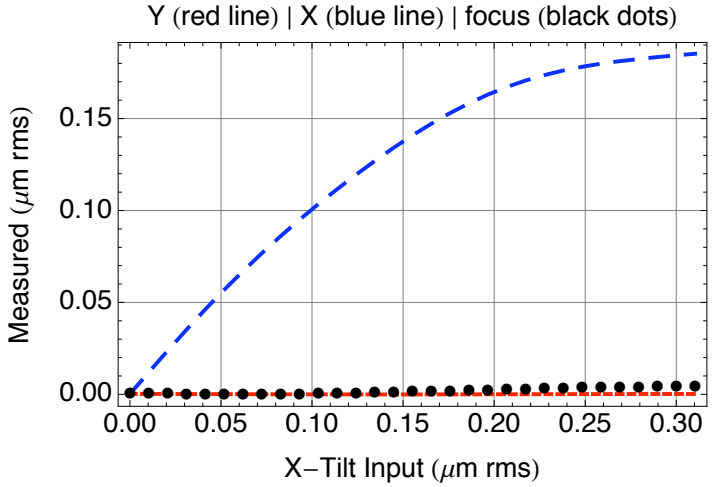

Figure 4. Measured Zernike coefficients for tilt and focus versus input tilt for a 4 sub-aperture Shack-Hartmann sensor in the absence of noise.

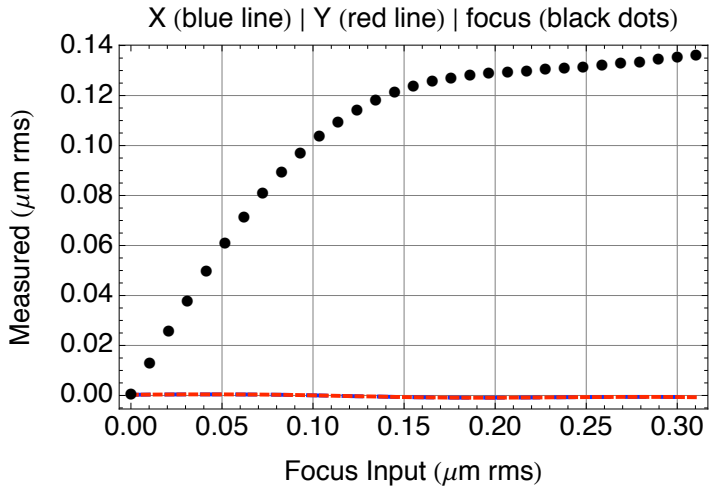

Figure 5. Measured Zernike coefficients for tilt and focus versus input focus for a 4 sub-aperture Shack-Hartmann sensor in the absence of noise.

Next, I examined the performance of the 4 sub-aperture Shack-Hartmann in the presence of noise. Figure 6 shows histograms for two situations with x-tilt input, low signal (12.5 electrons) and high signal (125 electrons).

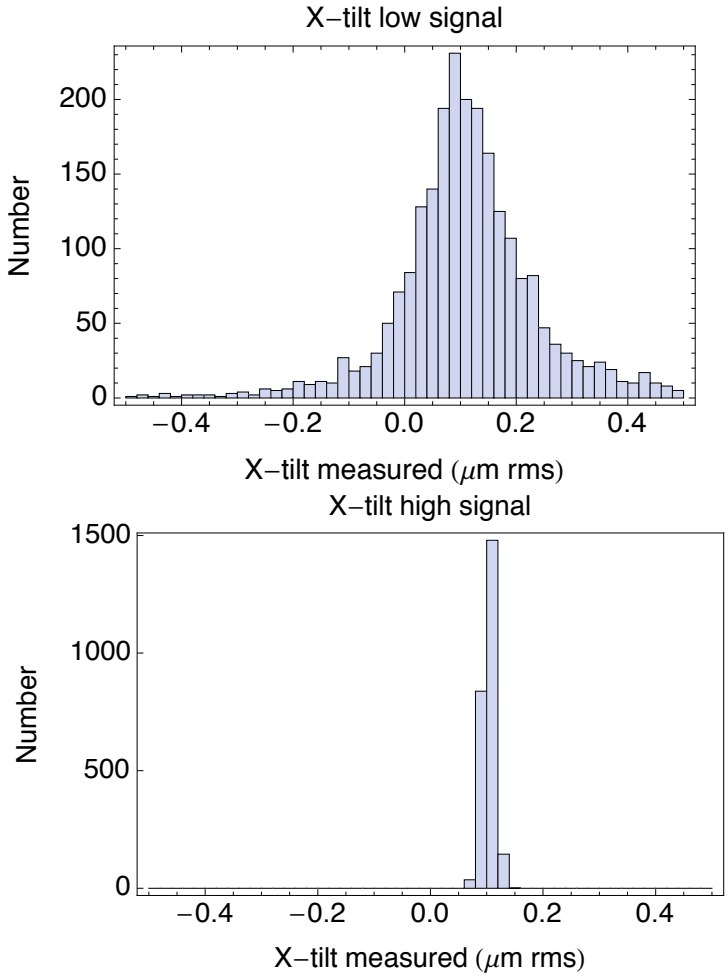

Figure 6. Histograms of Zernike x-tilt input of 0.1 μm rms for low signal (12.5 e^-) and high signal (125 e^-) for a 4 sub-aperture Shack-Hartmann sensor with a read noise of 3 electrons.

Figure 7 shows histograms for two situations with focus input, low signal (12.5 electrons) and high signal (125 electrons). In both the tilt and focus measurements, the background noise is zero, as would be appropriate for a cooled silicon sensor that is integrating for 0.5 milliseconds. The read noise was 3 electrons, which is typical for a charge-coupled device (CCD) running at very low pixel rates. Read noise for an avalanche photodiode (APD) array operating in geiger mode would be zero. The distribution of both the tilt and focus measurements appears gaussian, with a width that depends on the amount of signal on the detector.

For a 12th magnitude object, we expect about 170 electrons total on the detector if it integrates for 0.5 milliseconds, which corresponds to 2000 frames per second. This assumes a wavelength range of 0.52 to 0.65 microns with a notch at 0.589 microns of 0.02 microns in width. The average transmission in this band is about 0.5. The sensor quantum efficiency was 0.45, which is consistent with our existing avalanche photodiode arrays.

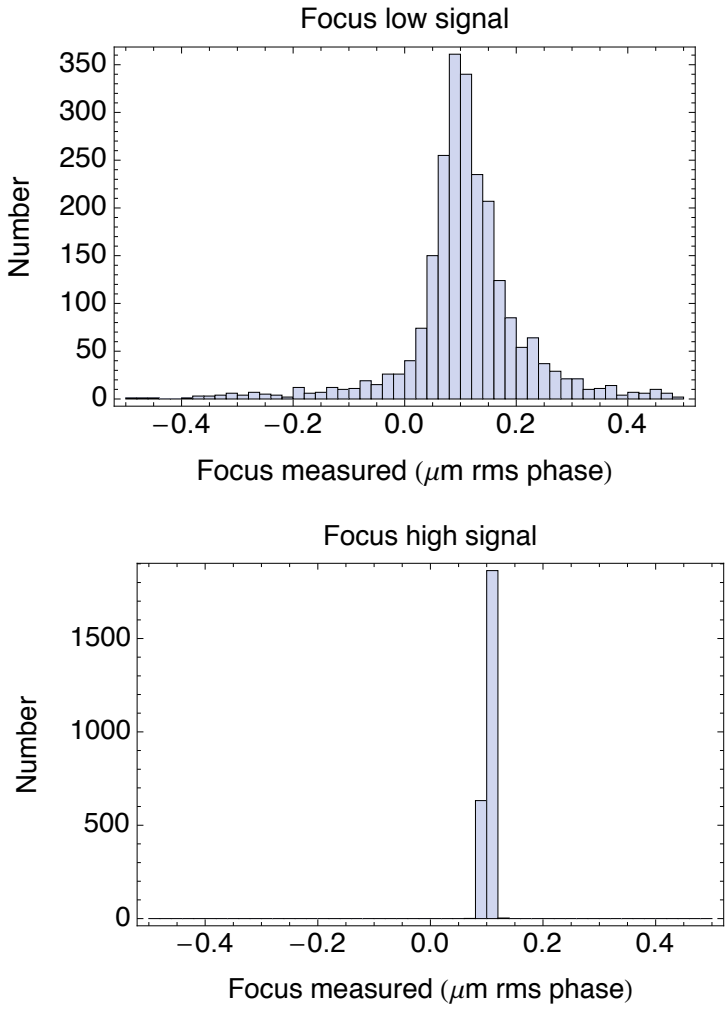

Figure 7. Histograms of focus input of 0.1 μm rms for low signal (12.5 e^-) and high signal (125 e^-) for a 4 sub-aperture Shack-Hartmann sensor with a read noise of 3 electrons.

I repeated the measurements shown in Figures 6 and 7 for a wide range of signal levels. Tilt measurements were made for a Zernike tilt input of 0.1 microns rms wavefront error and statistics were collected for 2500 realizations of detector noise. These results are plotted in Figure 8; previous results for a quad-cell are shown for comparison.

The tilt measurement error decreases rapidly up to about 125 electrons of signal, then it decreases more slowly. At low signal levels, where read noise dominates, the quad-cell out performs the 4 sub-aperture Shack-Hartmann sensor. At higher signal levels, where shot noise dominates, the 4 sub-aperture Shack-Hartmann sensor is superior in measuring Zernike tilt.

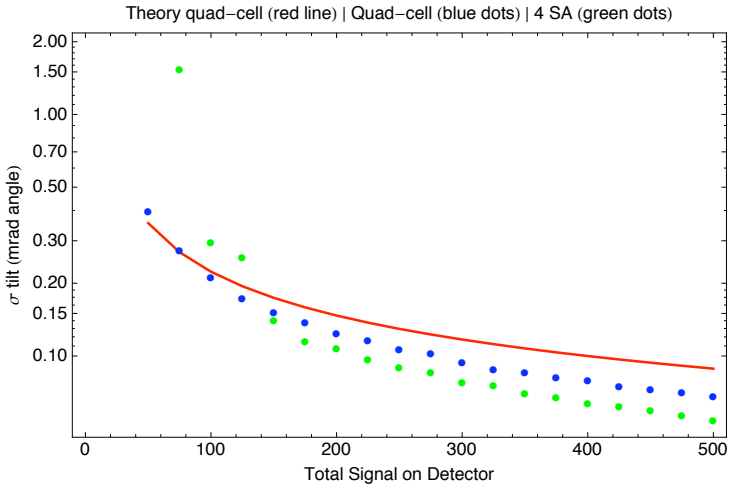

Figure 8. Zernike tilt measurement error versus total signal in electrons on the detector for a 4 sub-aperture Shack-Hartmann sensor with a read noise of 3 electrons; similar results for a quad-cell are shown for comparison.

Next, I made estimates of focus measurement error for the 4 sub-aperture Shack-Hartmann sensor. As before, there were 2500 realizations of detector read noise of 3 electrons. As with tilt measurement error, the focus measurement error decreases rapidly up to 150 electrons, then it decreases more slowly as the signal on the detector is increased.

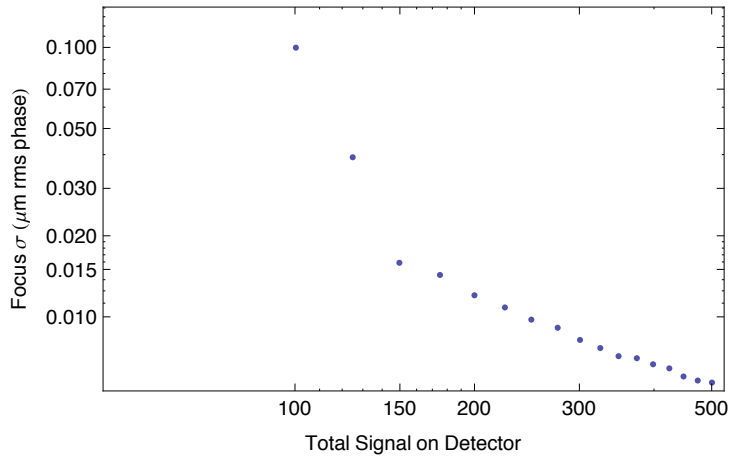

Figure 8. Focus measurement error versus total signal in electrons on the detector for a 4 sub-aperture Shack-Hartmann sensor with a read noise of 3 electrons.

5. CONCLUSION

This preliminary work shows the feasibility of using a 4 sub-aperture Shack-Hartmann sensor for measuring both tilt and focus. The same measurements could be made using 3 hexagonal-shaped lenslets, which would use the available light more efficiently. We will investigate this idea further, but it is difficult to align an array of detector elements arranged on a rectangular grid to an array of hexagonal-shaped lenslets.

I plan to extend this work modeling the new optical design for this sensor. I also will make a comparison of CCD versus APD performance as detector arrays for this application. For the APD array, I will include the effects of crosstalk from adjacent pixels. I also may implement different reconstructors to extract tilt and focus from the measurements in the presence of atmospheric turbulence. Finally, we plan to build a prototype sensor in the laboratory and integrate it with optics to mimic the environment on the telescope. This will provide a wealth of information to help reinforce the feasibility of this scheme.

6. REFERENCES

1. Summers D., et al, Focus and pointing adjustments necessary for laser guide star adaptive optics at the W. M. Keck Observatory, *SPIE Astronomical Telescopes and Instrumentation Conference*, Glasgow, Scotland, 21–25 June 2004.
2. Link D. and Foucault B., Investigation of focus control for NGAS, Starfire Optical Range internal memo, 8 May 2007.
3. Goodman J., *Introduction to Fourier Optics*, McGraw-Hill, New York, 2nd ed., 1996.
4. Roggemann M. and Schulz T., Algorithm to increase the largest aberration that can be reconstructed from Hartmann sensor measurements, *Appl. Opt.* 37, pp. 4321–4329, 1998.
5. Noll R., Zernike ploynomials and atmospheric turbulence, J. Opt. Soc. Am., 66, pp. 207–211, 1976.
6. Tyler G. and Fried D., Image-position error associated with a quadrant detector, J. Opt. Soc. Am., Vol. 72, No. 6, June 1982.
7. Hardy J., *Adaptive Optics for Astronomical Telescopes*, Oxford University Press, Oxford, 1998.